

Theoretical model of the Leidenfrost temperature

Sergey Gavrilyuk¹ and Henri Gouin^{1*}

¹*Aix Marseille University, CNRS, IUSTI, UMR 7343, Marseille, France**

The *Leidenfrost effect* is a phenomenon in which a liquid, poured onto a glowing surface significantly hotter than the liquid's boiling point, produces a layer of vapor that prevents the liquid from rapid evaporation. Rather than making physical contact, a drop of water levitates above the surface.

The temperature above which the phenomenon occurs is called the *Leidenfrost temperature*. The reason for the existence of the Leidenfrost temperature, which is much higher than the boiling point of the liquid, is not fully understood and predicted. For water we prove that the Leidenfrost temperature corresponds to a bifurcation in the solutions of equations describing evaporation of a nonequilibrium liquid–vapor interface. For water, the theoretical values of obtained Leidenfrost temperature, and that of the liquid–vapor interface which is smaller than the boiling point of liquid, fit the experimental results found in the literature.

PACS Numbers: 05.70-a; 05.70.Ln; 05.70.Np; 05.70.Fh

Keywords: Leidenfrost effect, boiling crisis, nonequilibrium thermodynamics, capillarity effect, dynamic interfaces.

I. INTRODUCTION

When water is projected onto a moderately heated metal plate, it spreads out, starts to boil and evaporates very quickly. Things are quite different when the metal is incandescent: the water temperature remains below the boiling temperature, divides into numerous droplets that roll, bounce and at the end of their life they either take-off or explode. These phenomena are well described in Refs. [1–10]. The observations also show that the droplets perform translational and rotational motions. These movements lead to geometrically beautiful patterns. Photographic and stroboscopic tools were then used to describe the experiments, but the effect can be seen with the naked eye. Such a phenomenon is qualitatively very well described in Refs. [11, 12]. An analytical model of these figures and movements has been proposed in Ref. [13].

This *Leidenfrost effect*, also called the boiling crisis, was carefully observed in 1756 by the German physician J. G. Leidenfrost. Leidenfrost had well understood the cause of the *film boiling* phenomenon: there is no contact between the glowing solid and water, the liquid evaporates in the vicinity of the solid and levitates on a cushion of steam [14].

In 1844, M. Boutigny had also experimented on himself some curious facts related to the phenomenon such as plunging his hand in a bath of molten iron without burning himself [15]. Fiery coal can reach about 540 degrees Celsius; candidates for walking on hot coals must moisten their feet to benefit from the Leidenfrost effect. At the end of the 19th century, physicists multiplied astonishing experiments like transforming water into ice by pouring it into a crucible containing sulphurous acid and heated to red hot [16].

Today, it is no longer these curiosities that are the subject of in-depth studies, a lot of new activities are rising about the Leidenfrost phenomenon. Besides the industrial applications involving high temperature processes, the Leidenfrost effect offers new opportunities in self-propelling drops, in

drag reduction, in the frictionless transport, in chemical reactors without borders, in heat engines, etc...[17–20]. The boiling crisis is often the first step in an explosive process that is generated by the contact of a hot surface and a liquid. If it is well dominated by metallurgists for the hardening of metals, it is not yet the case in other fields where it is the cause of important accidents. For example, in the oil industry, at the bottom of the distillation towers is oil at a temperature of about 400 degrees Celsius. In these towers, very dry steam is injected at the same temperature. When, due to a malfunction in the installation, liquid water is injected, the explosion that occurs is so violent that it destroys most of the distillation plates [21]. In nuclear industry, several accidents were initiated by the phenomenon. In 1961, for the American SL-1 reactor at Idaho State Laboratory, an unexpected lifting of a control bar caused water to be projected over the core onto the vessel which, despite its weight of 13 tons, sheared the pipes to which it was connected and rose about 3 meters. In 1986, the boiling crisis phenomenon occurred in Chernobyl, and in 2011 in Fukushima, creating major nuclear accidents. The largest terrestrial explosion ever recorded, that of the Krakatoa volcano (in 1883) corresponding to 200 megatons of TNT, is also due to the contact of lava at high temperature with sea water.

These events have given rise to a large number of studies [22–26]. Of particular interest is the Leidenfrost temperature i.e., the temperature above which the phenomenon occurs. It depends on physico–chemical and mechanical properties of the heated surface, the liquid type and the ambient conditions [27, 28]. However, it cannot be said that a theory for a satisfactory prediction of the Leidenfrost temperature has been given. The Leidenfrost effect still retains an essential mystery about the reason for a temperature above which there is the creation of the vapor film. One may wonder why, under normal atmospheric pressure, the creation of the film does not occur at a temperature close to 100 degrees Celsius, the boiling temperature of water, which creates a large quantity of vapor.

* E-mails:sergey.gavrilyuk@univ-amu.fr henri.gouin@univ-amu.fr

In order to treat the problem as simply as possible, we consider a thin layer of liquid water on a flat, infinite and horizontal solid surface W at a uniform temperature T_w . The surface is ideal: it has no additional physico-chemical properties. Since the layer is thin, we can neglect the gravitational forces. A schematic description of such a *thought experiment* is shown in Fig. 1. The liquid water layer (a) is assumed to be separated from the water vapor layer by a liquid–vapor interface (i). We assume that the liquid water layer is under atmospheric pressure p_0 , and that the liquid–vapor interface is at temperature T_i . The vapor layer between the liquid–vapor interface (i) and the heated surface W is decomposed into two parts: an intermediate part (b) where the temperature varies from T_i to T_w , and the part (c) at temperature T_w where the vapor is evacuated along the solid surface W . It has been observed that the boiling crisis is always accompanied by a specific frequency regime called in the literature *1/f – noise* (see Ref. [23] and references therein). We assume that the vapor density oscillations immediately appear near the interface and disappear at the end of the part (b). We only need to model the phase transition at the interface (i) and non-isothermal and non-homogeneous one–dimensional vapor flow in (b). For (b), we use a phase-field model [29, 30]. It allows us to find the *bifurcation temperature* below which the existence of such a configuration is not possible. Without claiming that our model will solve all the problems posed by the boiling crisis, we believe that it can help to understand the phenomenon by explaining for water the origin of the Leidenfrost temperature.

To simplify the presentation of the article, we have separate the paper into six sections and three appendices. In section II we present the classical van der Waals equation of state and its adjustment to our problem. Section III studies the thermo-mechanical van der Waals–Korteweg model across the liquid–vapor interface and in the vapor part of the flow. Sections IV and V study the dimensionless governing equations of one-dimensional flows. In Section VI the numerical calculations of the governing equations are performed related to experimental data to obtain the Leidenfrost temperature value. A conclusion ends this presentation. Some technical details are shown in Appendices A, B and C.

II. THE VAN DER WAALS EQUATION OF STATE

We adapt to our problem the simplest model for the description of equilibrium liquid–vapor interfaces for water: the van der Waals equation of state. Experimental values of physical quantities for water at the boiling temperature $T_0 = 373.15$ Kelvin (corresponding to 100 degrees Celsius) are presented in International System of Units (SI) (see [31]):

$$p_0 \approx 101325 \text{ Pa}, \quad v_g \approx 1.673 \text{ m}^3/\text{kg}, \quad v_l \approx 0.001043 \text{ m}^3/\text{kg},$$

where p_0 is the atmospheric pressure, v_g and v_l are specific volumes of vapor and liquid water at phase equilibrium, respectively. Here and in what follows, we use the SI system.

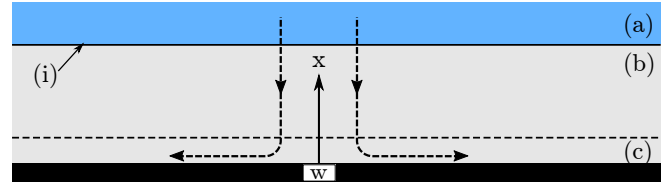


FIG. 1. Sketch of a quasi-one-dimensional transverse fluid flow. Domain (a) is a thin liquid layer; (i) is the liquid–vapor discontinuity interface which is a very thin region of few nanometers thickness of vapor having the temperature T_i ; domain (b) is the non-isothermal part of the vapor flow; the temperature increases from T_i to T_w . Region (c) is the part of the vapor region where the flow is not one–dimensional: the vapor escapes along the solid surface. The arrows show the flow direction.

The van der Waals equation of state is

$$p = \frac{RT}{v-b} - \frac{a}{v^2}, \quad (1)$$

where a, b, R are constant, $v = 1/\rho$ is the specific volume, and ρ is the density. When v is large, the van der Waals equation (1) yields the equation of state of perfect gas $p v = RT$. At a given temperature T , one obtains the chemical potential μ (defined up to an additive constant), where $d\mu = v dp$:

$$\mu(v, T) = -RT \text{Log}(v-b) + \frac{RTb}{v-b} - \frac{2a}{v}. \quad (2)$$

The van der Waals equation of state depends on two coefficients a and b and is considered as a good qualitative approximation for the description of equilibrium phase transitions. However, for a given temperature, Maxwell’s rule cannot be satisfied because we have to solve three scalar equations with two unknown scalars a and b . Instead of using a more complicated virial form of the equation of state with a large number of temperature dependent coefficients (cf. Refs. [32, 33]), we adopt a different approach. Rather than the perfect gas constant, we consider a new adaptable parameter. This simplifies our theoretical approach. To avoid confusion, we write \mathcal{R} instead of R in Eqs. (1) and (2).

To adapt Eq. (1) to our problem, we calculate the values of a, b and \mathcal{R} to satisfy the mechanical and chemical equilibrium at atmospheric pressure p_0 . The equilibrium Maxwell conditions of liquid–vapor interface are

$$\left\{ \begin{array}{l} \frac{\mathcal{R}T_0}{v_g-b} - \frac{a}{v_g^2} = \frac{\mathcal{R}T_0}{v_l-b} - \frac{a}{v_l^2} = p_0, \\ \mu(v_g, T_0) = \mu(v_l, T_0). \end{array} \right. \quad (3)$$

At $T_0 = 373.15$ K (100°C), we obtain

$$a \approx 1.52 \times 10^3 \text{ m}^5 \text{ s}^{-2}, \quad b \approx 9.2 \times 10^{-4} \text{ m}^3 \text{ kg}^{-1},$$

$$\mathcal{R} \approx 456 \text{ m}^2 \text{ s}^{-2} \text{ K}^{-1}.$$

The obtained values of a and b are thus different from those calculated for the thermodynamic critical point [33]. However, the value of \mathcal{R} is close to that of the perfect gas constant

which is $R = 462 \text{ m}^2 \text{ s}^{-2} \text{ K}^{-1}$. We define a characteristic specific volume v_0 of the vapor phase as:

$$p_0 v_0 = \mathcal{R} T_0,$$

which gives

$$v_0 \approx 1.68 \text{ m}^3 \text{ kg}^{-1}.$$

Van der Waals' model is a qualitatively realistic equilibrium model even far from the boiling point. Indeed, when we consider vapor and liquid water near 160°C , we obtain from system (3) other values of coefficients a , b and \mathcal{R} :

$$a \approx 1.40 \times 10^3 \text{ m}^5 \text{ s}^{-2}, \quad b \approx 9.3 \times 10^{-4} \text{ m}^3 \text{ kg}^{-1},$$

$$\mathcal{R} \approx 447 \text{ m}^2 \text{ s}^{-2} \text{ K}^{-1}.$$

Even the values of a , b vary with the temperature, their effect on the pressure variation is smaller than 0.5%. The variation of \mathcal{R} gives an error in the pressure value smaller than 2%. For the numerical calculations, we use

$$a \approx 1.49 \times 10^3 \text{ m}^5 \text{ s}^{-2}, \quad b \approx 9.2 \times 10^{-4} \text{ m}^3 \text{ kg}^{-1},$$

$$\mathcal{R} \approx 456 \text{ m}^2 \text{ s}^{-2} \text{ K}^{-1}.$$

The coefficient a corresponding to the molecular attraction is smaller than the one for classical equilibrium at 100°C .

III. A CONTINUOUS THEORY OF CAPILLARITY

We now introduce the second gradient theory of fluids where the internal energy depends on density gradients [34, 35]. In fact, such a model is a special case of the Cahn and Hilliard phase field model [29]. It has been developed, in particular, by Rowlinson and Widom [30].

The second gradient theory, conceptually more straightforward than the Laplace theory, can be used to construct a continuous theory for fluid interfaces. Rowlinson and Widom wrote: *the view that the interfacial region may be treated as matter in bulk, with a local free-energy density that is that of hypothetically uniform fluid of composition equal to the local composition, with an additional term arising from the non-uniformity, and that the latter may be approximated by a gradient expansion typically truncated in second order; is then most likely to be successful and perhaps even quantitatively accurate.* The essential difference compared to classical compressible fluids is that the specific internal energy depends not only on the density $\rho = 1/v$, specific entropy η , but also of $\nabla\rho$. The specific internal energy α characterizes both the compressibility and capillarity properties of the fluid. Due to fluid isotropy, this energy depends only on the norm of density gradient. The simplest expression of the specific energy is:

$$\alpha = \varepsilon(\rho, \eta) + \frac{\lambda}{2\rho} |\nabla\rho|^2, \quad \lambda = \text{const} > 0. \quad (4)$$

Here $\varepsilon(\rho, \eta)$ is the classical specific energy and λ is a *capillarity coefficient* which is related to the surface tension coefficient:

The relation between the surface tension γ and coefficient λ is given explicitly in Ref. [30] (chapter 3, pages 50–57). In appropriate CGS units more adapted to capillary phenomena, the value of λ is of order 10^{-5} , its dimension is $[\text{g}]^{-1} [\text{cm}]^7 [\text{s}]^{-2}$. It can be calculated as (formula (3.11) in Ref. [30]):

$$\gamma = \int_{-\infty}^{+\infty} \lambda \left(\frac{d\rho}{dz} \right)^2 dz = \int_{\rho_v}^{\rho_l} \lambda \frac{d\rho}{dz} d\rho,$$

where z is the distance in the direction normal to the interface. It can be approximately written as:

$$\lambda \approx \frac{\gamma h}{(\rho_l - \rho_v)^2}$$

where h is the thickness of the interface, and ρ_l and ρ_v are the densities of the liquid and vapor, respectively.

Such a gradient density dependent energy appears in the case of large density fluctuations [36]. This is not classical equilibrium thermodynamics of homogeneous states, but thermodynamics of non-homogeneous states. Compared to the classical Laplace theory, the second gradient theory reveals a microstructure of the liquid-vapor interface. Experimental studies of this microstructure have been carried out by the schools of Derjaguin and de Gennes [37, 38].

A. Conservative motion

For conservative motion, the van der Waals–Korteweg equations of non-homogeneous capillary fluids can be derived from the *Hamilton principle of stationary action* by using the well-known Lagrangian [39–42]:

$$\mathcal{L} = \rho \left(\frac{|\mathbf{u}|^2}{2} - \alpha - \Omega \right),$$

where \mathbf{u} is the velocity, Ω is the specific potential of external forces, and α is given by Eq. (4). The usual constraints are the mass and entropy conservation laws:

$$\frac{\partial\rho}{\partial t} + \text{div}(\rho \mathbf{u}) = 0, \quad (5)$$

and

$$\frac{\partial\rho\eta}{\partial t} + \text{div}(\rho\eta \mathbf{u}) = 0. \quad (6)$$

We refer to calculations in Refs. [34, 35, 43] to directly write the momentum equations in the form:

$$\frac{\partial\rho \mathbf{u}}{\partial t} + \text{div}(\rho \mathbf{u} \otimes \mathbf{u} - \boldsymbol{\sigma}) + \rho \nabla \Omega = \mathbf{0}, \quad (7)$$

where

$$\boldsymbol{\sigma} = - \left(p - \frac{\lambda}{2} |\nabla\rho|^2 - \lambda \rho \Delta\rho \right) \mathbf{I} - \lambda \nabla\rho \otimes \nabla\rho,$$

$$p = \rho^2 \frac{\partial\varepsilon(\rho, \eta)}{\partial\rho},$$

where I is the unit tensor. Due to a small thickness of the fluid layer, gravitational forces are neglected. As a consequence of Eqs. (5), (6) and (7), one obtains the energy equation :

$$\frac{\partial e}{\partial t} + \text{div} \left(e\mathbf{u} - \boldsymbol{\sigma}\mathbf{u} - \lambda \frac{d\rho}{dt} \nabla \rho \right) = 0, \quad e = \rho \left(\frac{|\mathbf{u}|^2}{2} + \alpha \right). \quad (8)$$

In the one-dimensional case, the x -axis is drawn perpendicular to the liquid layer and heated surface (see Fig. 1). The governing Eq. (7) is written as:

$$\frac{\partial}{\partial t}(\rho u) + \frac{\partial}{\partial x}(\rho u^2 + P) = 0, \quad (9)$$

where

$$P = p + k, \quad \text{with} \quad k = \frac{\lambda}{2} \left(\frac{\partial \rho}{\partial x} \right)^2 - \lambda \rho \frac{\partial^2 \rho}{\partial x^2}. \quad (10)$$

Here t denotes the time, x the space variable perpendicular to the liquid layer and glowing surface, u is the corresponding scalar velocity. Note that P can be considered as a total pressure: it is the sum of the thermodynamic pressure p and *capillary pressure part* k . If k is positive (negative), then $P > p$ ($P < p$). In the one-dimensional case, Eq. (7) writes

$$\frac{\partial(\rho u)}{\partial t} + \frac{\partial}{\partial x} \left(\rho u^2 + p(\rho, T) + \frac{\lambda}{2} \left(\frac{\partial \rho}{\partial x} \right)^2 - \lambda \rho \frac{\partial^2 \rho}{\partial x^2} \right) = 0$$

At constant temperature T , the Gibbs relation becomes $dp/\rho = d\mu$. Then, using conservation of mass, one obtains

$$\rho \left(\frac{\partial u}{\partial t} + u \frac{\partial u}{\partial x} \right) + p'(\rho) \frac{\partial \rho}{\partial x} - \lambda \rho \frac{\partial^3 \rho}{\partial x^3} = 0,$$

or

$$\frac{\partial u}{\partial t} + u \frac{\partial u}{\partial x} + \frac{\partial \mu}{\partial x} - \lambda \frac{\partial^3 \rho}{\partial x^3} = 0.$$

Thus, at a given temperature T , Eq. (9) admits the conservation law:

$$\frac{\partial u}{\partial t} + \frac{\partial}{\partial x} \left(\frac{u^2}{2} + \mu(\rho, T) - \lambda \frac{\partial^2 \rho}{\partial x^2} \right) = 0 \quad (11)$$

associated with chemical potential μ (a particular case of μ from Eq. (2) is calculated for the van der Waals equation of state).

Depending on other additional constraints (isothermal or isobaric processes), we consider the chemical potential or the specific enthalpy instead of the specific internal energy (the details are further explained in Appendices B 1 and B 2).

B. One-dimensional stationary vapor motion

In the rest of the paper, one supposes that the consumed liquid is fed by an external pump that allows the motion to

be steady. We assume one-dimensional flow in the x direction of the domain (b) (see Fig. 1). The viscosity is negligible because the evaporation process is very slow. In the one-dimensional stationary case, Eq. (5) yields:

$$\rho u = q, \quad q = \text{const}, \quad (12)$$

where q represents the constant flow rate of the fluid.

Equation (9) writes:

$$\frac{d}{dx}(\rho u^2 + P) = 0, \quad (13)$$

• Through the liquid-vapor interface, Eq. (9) implies the jump condition:

$$[P + q^2 v] = 0,$$

i.e.

$$P_i - p_0 + q^2(v_{g_i} - v_{l_i}) = 0, \quad (14)$$

where the index i refers to the interface: $v_{l_i} = 1/\rho_{l_i}$ ($v_{g_i} = 1/\rho_{g_i}$) the liquid (vapor) specific volume at interface (i), P_i is the total pressure in the vapor phase on the interface, and p_0 is the pressure in the liquid bulk on the interface, and the square brackets mean the difference of values across interface (i). Since the liquid layer is thin, the gravity is not taken into account, thus the interface liquid thermodynamic pressure is the atmospheric pressure p_0 .

• In domains (b), we obtain from Eq. (13):

$$P_i - p_w + q^2(v_{g_i} - v_w) = 0,$$

where the index w corresponds to the heated surface W . The vapor on the boundary between (b) and (c) is assumed to be homogeneous of specific volume v_w and temperature T_w . Thus, the total pressure is only the thermodynamic pressure part p_w . The difference with Eq. (14) yields:

$$p_w - p_0 + q^2(v_w - v_{l_i}) = 0. \quad (15)$$

• The conservation law (11) yields the jump relation through the isothermal liquid-vapor interface:

$$\left[\frac{u^2}{2} + \mu(\rho, T_i) - \lambda \frac{d^2 \rho}{dx^2} \right] = 0, \quad (16)$$

where $\mu(\rho, T_i)$ is defined by Eq. (2). Equation (16) can be considered as a dynamical Maxwell rule (see also Appendix B 1).

• The vapor motion in domain (b) is not isothermal. The viscosity of the vapor phase is negligible, so the equation of motion (13) is unchanged. The equation of the energy balance (8) in the vapor phase must take into account the heat exchange in the vapor region. Such a balance equation is in

the form:

$$\left\{ (e + P)u - \lambda \left(\frac{d\rho}{dx} \right)^2 u \right\}_{|\rho_{g_i}, T_i} - \left\{ (e + P)u - \lambda \left(\frac{d\rho}{dx} \right)^2 u \right\}_{|\rho_w, T_w} = \dot{Q}_w - \dot{Q}_i. \quad (17)$$

Compared to Eq. (8), we added in the total energy the balance of heat fluxes $\dot{Q}_w - \dot{Q}_i$. Also, since the flow volume is fixed, it changes the expression of e (for proof, see Appendix B 2):

$$e = \rho(u^2/2 + \mathcal{H}) \quad \text{with} \quad \mathcal{H} = H + \frac{\lambda}{2\rho} \left(\frac{d\rho}{dx} \right)^2, \quad H = \varepsilon + \frac{p_0}{\rho}.$$

Thus, \mathcal{H} is the specific enthalpy of capillary fluid at pressure p_0 , and H is the enthalpy of a homogeneous fluid at pressure p_0 . The expression of P is given by Eq. (10). In the domain (c) near the surface W the density becomes homogeneous and the balance law (17) becomes

$$\left\{ (e + P)u - \lambda \left(\frac{d\rho}{dx} \right)^2 u \right\}_{|\rho_{g_i}, T_i} - \{(e + P)u\}_{|\rho_w, T_w} = \dot{Q}_w - \dot{Q}_i. \quad (18)$$

The vapor density strongly varies near and through the interface.

At the interface, considered as a discontinuity, an extra condition must be added on both sides of the interfacial discontinuity:

$$\frac{d\rho}{dx} = 0. \quad (19)$$

The additional condition (19) called also *Weierstrass-Erdmann condition* is fundamental in the rest of our paper. It is recalled and explained in Appendix A. Also, condition (19) is obtained and analyzed in [41, 44, 45]. Physically, it means the absence of microenergy concentration at the surface of discontinuity. Such a condition also appears when a capillary fluid is in contact with a surface when the surface is neither attractive or repulsive [37, 46].

The density jump implies $d^2\rho/dx^2 < 0$, and consequently, due to (10), $k > 0$ (this property is analyzed in Fig. 8 upper diagram of Appendix C).

The vapor at temperature T_w is assumed to be homogeneous. Using relation (18) complemented by Eq. (19), we get

$$\begin{aligned} & \frac{1}{2} \frac{q^3}{\rho_i^2} + p_i v_{g_i} q - \lambda \frac{d^2\rho_{g_i}}{dx^2} q + H_i q + \dot{Q}_i \\ & = \frac{1}{2} \frac{q^3}{\rho_w^2} + p_w v_w q + H_w q + \dot{Q}_w. \end{aligned}$$

Here indices “ i ” and “ w ” mean values of variables at the interface and surface, respectively. In the above relation the second

derivative of the density ρ_{g_i} is *a priori* - non-vanishing.

Since $k = -\lambda\rho_{g_i} \frac{d\rho_{g_i}^2}{dx^2}$ and $P_i = p_i + k$, we get:

$$\frac{1}{2} q^2 v_{g_i}^2 + H_i + P_i v_{g_i} + \frac{\dot{Q}_i}{q} = \frac{1}{2} q^2 v_w^2 + H_w + p_w v_w + \frac{\dot{Q}_w}{q}. \quad (20)$$

Let us underline that:

$$p_i = p(v_{g_i}, T_i), \quad p_w = p(v_w, T_w).$$

From Eq. (1), we have [33]:

$$\varepsilon = \int c_v(T) dT - \frac{a}{v},$$

where $c_v(T)$ is the specific heat of water vapor at constant volume. Equation (20) implies:

$$\begin{aligned} & \frac{1}{2} q^2 (v_{g_i}^2 - v_w^2) + \int_{T_w}^{T_i} c_v(T) dT + 2k v_{g_i} \\ & + 2 \left(\frac{\mathcal{R}T_i v_{g_i}}{v_{g_i} - b} - \frac{\mathcal{R}T_w v_w}{v_w - b} \right) - \frac{a}{v_{g_i}} + \frac{a}{v_w} + \frac{\dot{Q}_i}{q} - \frac{\dot{Q}_w}{q} = 0. \end{aligned} \quad (21)$$

We approximate the vapor equation of state by $p_i v_{g_i} \approx \mathcal{R}T_i$, $p_w v_w \approx \mathcal{R}T_w$, and introduce

$$c_p(T) = c_v(T) + \mathcal{R},$$

corresponding to the specific heat at constant pressure which depends only on temperature T . We obtain from Eq. (21):

$$\begin{aligned} & \frac{1}{2} q^2 (v_{g_i}^2 - v_w^2) + \int_{T_w}^{T_i} c_p(T) dT + 2k v_{g_i} \\ & + \mathcal{R}(T_i - T_w) + \frac{\dot{Q}_i}{q} - \frac{\dot{Q}_w}{q} = 0, \end{aligned} \quad (22)$$

To transform a liquid into saturated vapor, we need to supply latent heat L . At a given temperature, and for the van der Waals equation of state, the energy of a saturated vapor is approximately independent on the pressure. Indeed, considering the internal energy as a function of v and T , one has:

$$\varepsilon(v_g, T) - \varepsilon(v_{g_s}, T) = a \left(\frac{1}{v_{g_s}} - \frac{1}{v_g} \right),$$

where v_{g_s} is the specific volume of saturated vapor at pressure p_s (index s means *saturated*), and v_g is the specific volume of vapor at pressure p_0 . Compared to the latent heat value, this variation is small even for a large variation of the specific volume of the vapor and we can thus assume that $\varepsilon(v_g, T) \approx \varepsilon(v_{g_s}, T)$. Let $L(T)$ be the specific heat of evaporation for saturated vapor (specific latent heat). One has:

$$L(T_i) - L(T_w) = (\varepsilon(v_{g_i}, T_i) + p_{si} v_{g_i}) - (\varepsilon(v_{g_w}, T_w) + p_{sw} v_{g_w}).$$

The saturated vapor equation of state being approximated as:

$$p_{si} v_{g_i} \approx \mathcal{R}T_i, \quad \text{and} \quad p_{sw} v_{g_w} \approx \mathcal{R}T_w.$$

Hence,

$$L(T_i) - L(T_w) \approx \varepsilon(v_{sg_i}, T_i) - \varepsilon(v_{sg_w}, T_w) + \mathcal{R}(T_i - T_w).$$

At atmospheric pressure, the water vapor equation of state can also be approximated as:

$$p_0 v_{g_i} \approx \mathcal{R}T_i, \quad \text{and} \quad p_0 v_{g_w} \approx \mathcal{R}T_w,$$

The specific latent heat is the amount of heat that must be supplied to a pure liquid, in our case water, to produce the phase transition. Thus

$$\frac{\dot{Q}_i}{q} - \frac{\dot{Q}_w}{q} = L(T_i) - L(T_w).$$

This is in agreement with [6, 47]. Thus, Eq. (22) yields:

$$\begin{aligned} \frac{1}{2} q^2 (v_{g_i}^2 - v_w^2) + \int_{T_w}^{T_i} c_p(T) dT + 2k v_{g_i} \\ + \mathcal{R}(T_i - T_w) + L(T_i) - L(T_w) = 0, \end{aligned} \quad (23)$$

IV. DIMENSIONLESS EQUATIONS OF MOTION

We now consider the dimensionless form of the governing equations. The dimensionless variables are denoted by the same letters but with an additive *tilde sign*. In particular, the van der Waals equation of state (1) in dimensionless form is

$$\tilde{p} = \frac{\tilde{T}}{\tilde{v} - \tilde{b}} - \frac{\tilde{a}}{\tilde{v}^2} \quad (24)$$

with

$$\tilde{a} = \frac{a}{p_0 v_0^2}, \quad \tilde{b} = \frac{b}{v_0}, \quad \tilde{T} = \frac{T}{T_0}, \quad \tilde{p} = \frac{p}{p_0}, \quad \tilde{v} = \frac{v}{v_0},$$

where p_0, T_0 are defined in Section II and v_0 is defined from $p_0 v_0 = \mathcal{R}T_0$. We also introduce the dimensionless variables associated with capillary pressure term, specific volumes and flow rate:

$$\tilde{P}_i = \frac{P_i}{p_0}, \quad \tilde{k} = \frac{k}{p_0}, \quad \tilde{v}_{g_i} = \frac{v_{g_i}}{v_0}, \quad \tilde{v}_{l_i} = \frac{v_{l_i}}{v_0}, \quad \tilde{q} = \frac{q}{q_0}$$

with $q_0 = \sqrt{\frac{p_0}{v_0}}$.

The equation (14) takes the following form:

$$\tilde{P}_i - 1 + \tilde{q}^2 (\tilde{v}_{g_i} - \tilde{v}_{l_i}) = 0,$$

The dimensionless flow rate \tilde{q} is very small. Indeed, when the solid surface temperature is close to the Leidenfrost temperature, the lifetime of liquid dramatically increases, typically by a factor of 500 associated with the existence of a vapor layer isolating the liquid bulk. For example, a millimeter liquid layer on a duralumin surface at 200°C is observed to float for more than a whole minute [6, 48, 49]. So, the fluid velocity due to the liquid evaporation is about

$1.7 \times 10^{-5} \text{ m s}^{-1}$, and the flow rate $q \approx 1.7 \times 10^{-2} \text{ kg m s}^{-1}$.

For $q_0 = \sqrt{\frac{p_0}{v_0}} \approx 245 \text{ kg m s}^{-1}$, one has $\tilde{q} \approx 7 \times 10^{-5} \ll 1$.

Consequently, we can neglect \tilde{q}^2 in the dimensionless governing equations.

The water vapor at pressure p_0 can be considered as a gas and we obtain from Eqs. (14) and (15):

$$p_w \approx P_i \approx p_0, \quad p_0 v_w \approx \mathcal{R}T_w.$$

In dimensionless form we get:

$$\tilde{v}_w \approx \tilde{T}_w \quad \text{and} \quad \tilde{P}_i \approx \tilde{p}_w \approx 1.$$

The pressure in vapor at temperature T_w is also the atmospheric pressure p_0 .

From $p_i v_{g_i} = \mathcal{R}T_i$, we obtain as a consequence of motion equation in domain (i):

$$\tilde{T}_i = \tilde{p}_i \tilde{v}_{g_i} = (\tilde{P}_i - \tilde{k}) \tilde{v}_{g_i} \quad \text{and} \quad \tilde{P}_i \approx 1. \quad (25)$$

Property:

Since $k > 0$ (see Appendix C), we must have $\tilde{T}_i/\tilde{v}_{g_i} < 1$. The limit case corresponds to:

$$\tilde{T}_i = \tilde{v}_{g_i}. \quad (26)$$

We hypothesize that the condition (26) defines the value of the Leidenfrost temperature. Indeed, as we have already mentioned, the total pressure P is composed of the thermodynamic pressure p and the capillary pressure term k . When k is positive, the thermodynamic pressure near the interface will be smaller than the atmospheric pressure in the vapor portion of the fluid. Therefore, the thermodynamic pressure gradient lifts the droplet. This lifting force can therefore be considered as a kind of Archimedean force (buoyancy force). In the following we will show that this hypothesis fits with experimental observations.

V. DIMENSIONLESS EQUATIONS OF ENERGY

A. Liquid–vapor interface (i)

The condition (16) across the liquid–vapor interface writes:

$$\frac{1}{2} q^2 v_{g_i}^2 + \mu(v_{g_i}, T_i) + k v_{g_i} = \frac{1}{2} q^2 v_{l_i}^2 + \mu(v_{l_i}, T_i),$$

and Eq. (2) yields:

$$\begin{aligned} \frac{1}{2} q^2 v_{g_i}^2 + k v_{g_i} - \mathcal{R}T_i \left\{ \text{Log} \left(\frac{v_{g_i} - b}{v_{l_i} - b} \right) - b \left(\frac{1}{v_{g_i} - b} - \frac{1}{v_{l_i} - b} \right) \right\} \\ + 2a \left(\frac{1}{v_{l_i}} - \frac{1}{v_{g_i}} \right) = 0. \end{aligned}$$

As proved in Section IV we can neglect \tilde{q}^2 and one obtains

$$\begin{aligned} & \tilde{k} \tilde{v}_{g_i} - \tilde{T}_i \left\{ \text{Log} \left(\frac{\tilde{v}_{g_i} - \tilde{b}}{\tilde{v}_{l_i} - \tilde{b}} \right) - \tilde{b} \left(\frac{1}{\tilde{v}_{g_i} - \tilde{b}} - \frac{1}{\tilde{v}_{l_i} - \tilde{b}} \right) \right\} \\ & + 2\tilde{a} \left(\frac{1}{\tilde{v}_{l_i}} - \frac{1}{\tilde{v}_{g_i}} \right) = 0. \end{aligned} \quad (27)$$

B. Non-isothermal vapor-layer (b)

For the specific heat at constant pressure c_p , we choose a quadratic model in temperature (see Fig. 2):

$$c_p(T) = K_1 + 2 K_2 T + 3 K_3 T^2. \quad (28)$$

By integration, we obtain:

$$\int_{T_w}^{T_i} c_p(T) dT = K_1 (T_i - T_w) + K_2 (T_i^2 - T_w^2) + K_3 (T_i^3 - T_w^3).$$

This is the custom to consider locally a linear approximation for $L(T)$ [50]:

$$L(T) = L_0 + L_1 T \quad \text{where} \quad L_1 < 0. \quad (29)$$

With Eqs. (28) and (29), Eq. (23) becomes:

$$\begin{aligned} & \frac{1}{2} \tilde{q}^2 (v_{g_i}^2 - v_w^2) + 2 k v_{g_i} + K_1 (T_i - T_w) + K_2 (T_i^2 - T_w^2) \\ & + K_3 (T_i^3 - T_w^3) + \mathcal{R} (T_i - T_w) + L_1 (T_i - T_w) = 0. \end{aligned} \quad (30)$$

Neglecting terms associated with \tilde{q}^2 , dimensionless form of Eq. (30) writes:

$$\begin{aligned} & 2\tilde{k} \tilde{v}_{g_i} + \tilde{K}_1 (\tilde{T}_i - \tilde{T}_w) + \tilde{K}_2 (\tilde{T}_i^2 - \tilde{T}_w^2) + \tilde{K}_3 (\tilde{T}_i^3 - \tilde{T}_w^3) \\ & + (\tilde{T}_i - \tilde{T}_w) + \tilde{L}_1 (\tilde{T}_i - \tilde{T}_w) = 0, \end{aligned} \quad (31)$$

where

$$\tilde{K}_1 = \frac{K_1}{\mathcal{R}}, \quad \tilde{K}_2 = \frac{K_2 T_0}{\mathcal{R}}, \quad \tilde{K}_3 = \frac{K_3 T_0^2}{\mathcal{R}}, \quad \tilde{L}_1 = \frac{L_1}{\mathcal{R}}.$$

T degrees Celsius	90°C	100°C	120°C	140°C	160°C	180°C	200°C
T Kelvin	363 K	373 K	393 K	413 K	433 K	453 K	473 K
c_p	2042.9	2080	2177	2310.9	2488.3	2712.9	2989.5

TABLE I. Isobaric heat capacity of water vapor is expressed in $J kg^{-1} K^{-1}$. The different temperature values are given together in degrees Celsius and Kelvin.

The following quadratic relation is used linking the heat capacity at constant pressure (in $J kg^{-1} K^{-1}$) as a function of

C. Consequences

In dimensionless form, Eq. (24) writes:

$$(\tilde{v}_{l_i} - \tilde{b}) \tilde{v}_{l_i}^2 - \tilde{T}_i \tilde{v}_{l_i}^2 + (\tilde{v}_{l_i} - \tilde{b}) \tilde{a} = 0. \quad (32)$$

Using Eqs. (25), one obtains:

$$\tilde{k} \tilde{v}_{g_i} = \tilde{v}_{g_i} - \tilde{T}_i. \quad (33)$$

Taking into account Eqs. (27), (31) and (32), and by using relation (33), the system allowing to solve our problem is:

$$\begin{cases} \tilde{v}_{g_i} - \tilde{T}_i - \tilde{T}_i \left\{ \text{Log} \left(\frac{\tilde{v}_{g_i} - \tilde{b}}{\tilde{v}_{l_i} - \tilde{b}} \right) - \tilde{b} \left(\frac{1}{\tilde{v}_{g_i} - \tilde{b}} - \frac{1}{\tilde{v}_{l_i} - \tilde{b}} \right) \right\} \\ + 2\tilde{a} \left(\frac{1}{\tilde{v}_{l_i}} - \frac{1}{\tilde{v}_{g_i}} \right) = 0, \\ 2 (\tilde{v}_{g_i} - \tilde{T}_i) + \tilde{K}_1 (\tilde{T}_i - \tilde{T}_w) + \tilde{K}_2 (\tilde{T}_i^2 - \tilde{T}_w^2) \\ + \tilde{K}_3 (\tilde{T}_i^3 - \tilde{T}_w^3) + (\tilde{T}_i - \tilde{T}_w) + \tilde{L}_1 (\tilde{T}_i - \tilde{T}_w) = 0, \\ \tilde{T}_i - (\tilde{v}_{l_i} - \tilde{b}) \left(\frac{\tilde{a}}{\tilde{v}_{l_i}^2} - 1 \right) = 0. \end{cases} \quad (34)$$

System (34) is a system of three equations relatively to unknowns $\tilde{v}_{g_i}, \tilde{v}_{l_i}, \tilde{T}_i$.

VI. NUMERICAL STUDY

A. Values of specific isobaric capacities of water vapor

The table, giving the values of specific isobaric capacities for water vapor, is taken from Refs. [31, 50].

the temperature T expressed in Kelvin:

$$c_p(T) = 8329 + 37.13 T - 0.05460 T^2. \quad (35)$$

T degrees Celsius	90°C	100°C	110°C	120°C	130°C	140°C	150°C	160°C	170°C	180°C	190°C	200°C
T Kelvin	363°K	373°K	383°K	393°K	403°K	413°K	423°K	433°K	443°K	453°K	463°K	473°K
L	2283.3	2256.4	2229.6	2202.1	2173.7	2144.3	2113.7	2082.0	2048.8	2014.2	1977.9	1939.7

TABLE II. The latent heat of liquid water to be transformed into vapor is expressed in $kJ\ kg^{-1}$. The different temperature values are given both in degrees Celsius and Kelvin.

T_w degrees Celsius	93.5°C	100°C	119°C	137°C	156°C	175°C	193°C	212°C
\tilde{T}_w	0.983	1	1.05	1.10	1.15	1.20	1.25	1.30
\tilde{v}_{g_i}	0.983	0.977	0.965	0.958	0.960	0.971	0.994	1.032
\tilde{T}_i	0.983	0.983	0.983	0.983	0.983	0.983	0.983	0.983
\tilde{v}_{l_i}	0.000621	0.000621	0.000621	0.000621	0.000621	0.000621	0.000621	0.000621

TABLE III. Calculations of \tilde{v}_{g_i} , \tilde{T}_i , \tilde{v}_{l_i} as a function of T_w by using the first linear approximation (36).

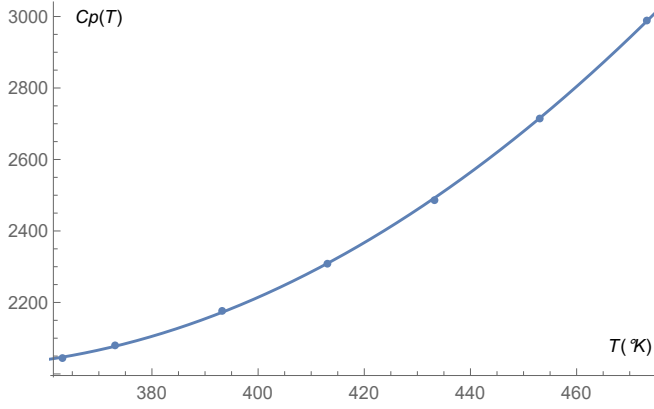


FIG. 2. Graph associated with experimental Table I and Eq. (35). The x axis indicates the Kelvin temperature, and the y axis indicates for water the corresponding isobaric heat capacity c_p expressed in $J\ kg^{-1}\ K^{-1}$. The dots represent c_p values coming from experimental Table I.

Then

$$\int_{T_w}^{T_i} c_p(T) dT = K_1 (T_i - T_w) + K_2 (T_i^2 - T_w^2) + K_3 (T_i^3 - T_w^3),$$

with

$$K_1 = 8329, \quad K_2 = 18.56, \quad K_3 = -0.01820.$$

Here and in the following, we do not indicate SI–dimensions of K_j coefficients $j \in \{1, 2, 3\}$. The experimental values of c_p are given in Table I. The corresponding approximation (35) is shown in Fig. 2. We see that relation (35) fits perfectly with experiment values.

B. Values of latent heat of vaporization for water

The table giving the values of latent heat of vaporization for water as a function of temperature is taken from [31, 50]. Usually, a local linear approximation of the latent heat $L(T)$

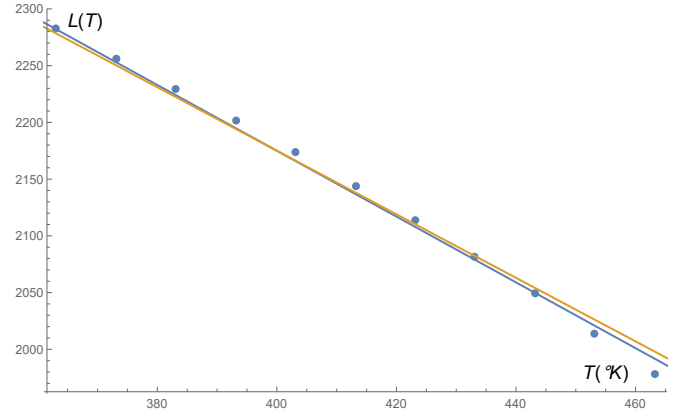


FIG. 3. The linear approximations of the latent heat of water in $kJ\ kg^{-1}$ expressed by Eq. (36) (in yellow) and Eq. (37) (in blue) are shown as functions of the Kelvin temperature. The dots represent the values of $L(T)$ from Table II.

in $kJ\ kg^{-1}$ (kilojoule per kilogram) is used as a function of temperature T expressed in Kelvin. We consider below two very close approximations of $L(T)$ to understand how the results obtained are sensitive to the values of the latent heat in the numerical calculations. Indeed, the data shown in Table II correspond to static measurements. In dynamics, the static latent heat is only a rough approximation: we do not take into account the heat radiation, physicochemical state and geometry of the heating surface, non-equilibrium process of evaporation, etc.

- First linear approximation:

$$L(T) = 3295 - 2.800 T \quad (36)$$

- Second linear approximation:

$$L(T) = 3385 - 2.900 T \quad (37)$$

These two close approximations are shown in Fig. 3. What matters is the difference of the latent heats $L(T_i)$ and

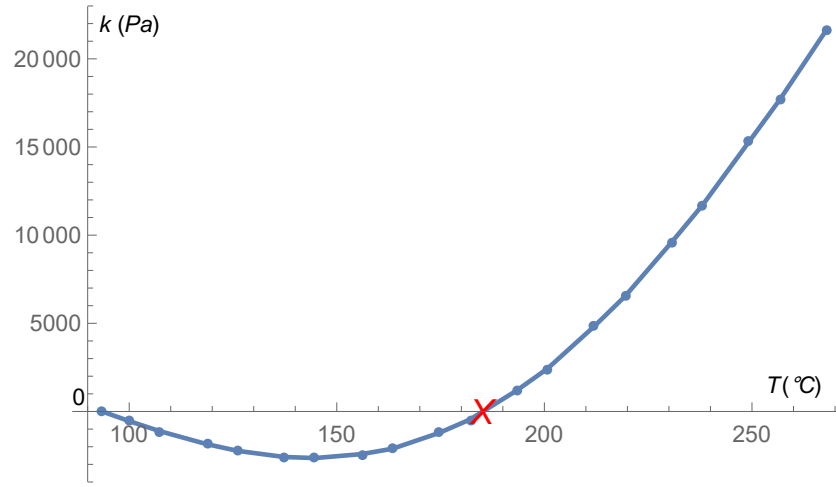


FIG. 4. Graphs associated with the k in Pa as a function of $T^{\circ}\text{C}$ in the *first linear approximation* (36). The x axis is associated with the Celsius temperature and the y axis with the pressure k expressed in Pascal. The dots represented k values calculated with the software *Mathematica*TM. In this case, the Leidenfrost temperature highlighted by a red cross is $T_L \approx 185^{\circ}\text{C}$.

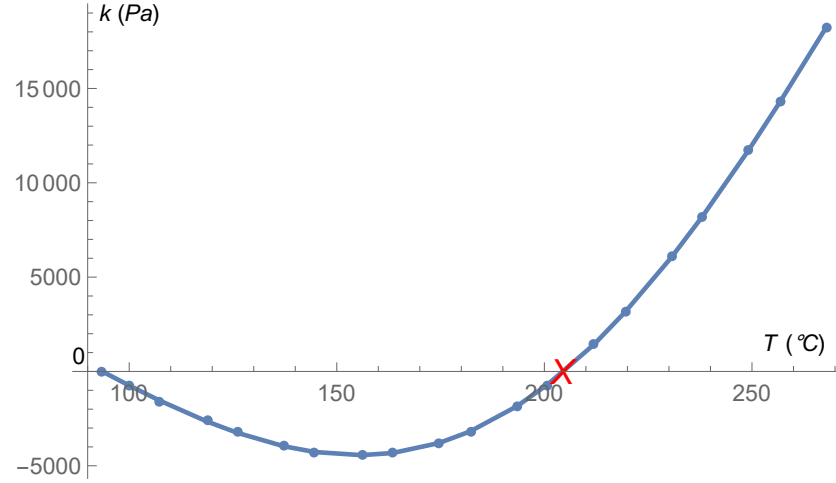


FIG. 5. Graphs associated with the k in Pa as a function of $T^{\circ}\text{C}$ in the *second linear approximation* (37). The x axis is associated with the Celsius temperature and the y axis with the pressure k expressed in Pascal. The dots represented k values calculated with the software *Mathematica*TM. In this case, the Leidenfrost temperature highlighted by a red cross is $T_L \approx 204^{\circ}\text{C}$.

T_w degrees Celsius	93.5°C	100°C	119°	137°C	156°C	175°C	193°C	212°C
\tilde{T}_w	0.983	1	1.05	1.10	1.15	1.20	1.25	1.30
$\tilde{\nu}_{g_i}$	0.983	0.975	0.958	0.946	0.941	0.947	0.965	0.997
\tilde{T}_i	0.983	0.983	0.983	0.983	0.983	0.983	0.983	0.983
$\tilde{\nu}_{l_i}$	0.000621	0.000621	0.000621	0.000621	0.000621	0.000621	0.000621	0.000621

TABLE IV. Calculations of $\tilde{\nu}_{g_i}$, \tilde{T}_i , $\tilde{\nu}_{l_i}$ as a function of T_w by using the second linear approximation (37) .

$L(T_w)$. Hence, only the slope in T is relevant. As we will

see, the variation of 3% of slopes between Eqs. (36) and (37), implies a sensible variation of the Leidenfrost temperature.

C. Calculations for water of Leidenfrost and interface temperatures

To show the sensitivity of results to the choice of model parameters. We have provided two close approximations of

the latent heat of evaporation to reveal the sensitivity of the

results with respect to these parameters.

For the first linear approximation (36) the corresponding Table III is formed. The condition $\tilde{v}_{gi} = \tilde{T}_i$ corresponds to the fact that k changes its sign. The value of T_w associated with bifurcation (26) is our definition of the Leidenfrost temperature which will be denoted by T_L . From Table III one can see that $\tilde{T}_i > \tilde{v}_{gi}$ at $\tilde{T}_w = 1.20$ but $\tilde{T}_i < \tilde{v}_{gi}$ at $\tilde{T}_w = 1.25$. At $\tilde{T}_w = \tilde{T}_L \approx 1.23$ one has $\tilde{T}_w = \tilde{v}_{gi}$. This critical value is the Leidenfrost temperature \tilde{T}_L . In this case, $T_L \approx 185^\circ\text{C}$.

For $T_w < T_L$ ($k < 0$) the liquid film sticks to the solid surface by causing the nucleate boiling. For $T_w > T_L$ ($k > 0$) the vapor film exists. In Fig. 4, we represent the value of k as a function of T_w in degrees Celsius.

For the second linear approximation (37) the corresponding Table IV is formed. The results are similar but the associated temperature corresponds to $\tilde{T}_L \approx 1.28$ i.e. $T_L \approx 204^\circ\text{C}$. On Fig. 5, we represent the value of k as a function of T_w .

The two approximations give noticeably different temperatures T_L (i.e. the variation of 3% of the slope of $L(T)$ implies the variation of 10% on T_L).

Let us note that when \tilde{T}_i is eliminated from the third equation of Eq. (34), only two equations for v_{li} and v_{gi} have to be solved. We show in Fig. 6 the intersection of the two corresponding curves for the the first linear approximation (36) and for the value of $\tilde{T}_w = 1.23$ corresponding to $T_w = 185^\circ\text{C}$.

In the literature, a wide range of values of Leidenfrost's temperature was measured [17]. The dispersion of values is related to the variation of experimental conditions (atmospheric conditions, deposition technics, drop size, thermal properties of the substrate, physico-chemical properties of the substrate surfaces (surface energy and roughness), method to characterize the transition, ...). Depending on the characteristics of the surface, the Leidenfrost temperature can be higher than $T_L \approx 204^\circ\text{C}$. We are not able to account for the various experimental conditions and have considered a flat, highly conductive solid substrate. However, the model provides a correct order of magnitude for the Leidenfrost temperature.

Moreover, it seems that, in the case of water, a minimum Leidenfrost temperature of about 150°C is observed for a liquid film on a flat, highly thermally conductive solid substrate [51, 52]. Nevertheless, it must be pointed out that experiments with ethanol drops on an oil basin can lead to a special Leidenfrost effect for a superheat as low as $T_L - T_0 = 1^\circ\text{C}$ relative to the boiling temperature. However, this technical feat has never been observed on a solid substrate [53].

Another important observation results in the computation of temperature T_i . Already Boutigny discovered that this temperature is lower than 100°C [15]. Experimental data predict a temperature of liquid bulk near the interface between 92° and 97°C [10, 54]. The temperature in the liquid bulk far from the interface depends on the shape of the drop and is linked to heat exchanges with the external environment. In our model, the obtained temperature of interface is $T_i \approx 93.5^\circ\text{C}$ corresponding to $\tilde{T}_i \approx 0.983$. For both approximations (36) and

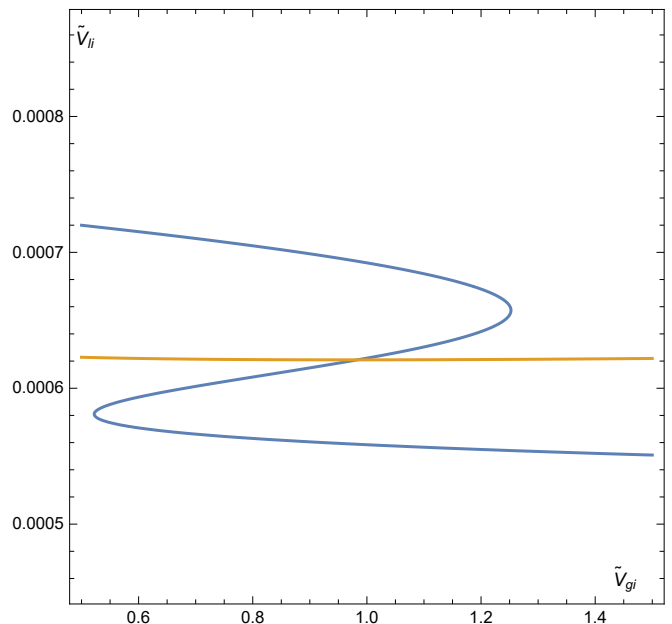


FIG. 6. Contour-graphs associated with the two first equations of system (34) are shown in the case $\tilde{T}_w = 1.23$, when \tilde{T}_i is eliminated from the third equation. The Z-shape curve corresponds to the Eq. (34)₂, the second curve corresponds to Eq. (34)₁. The horizontal (vertical) axis indicates dimensionless vapor and liquid specific volumes, respectively. The curves intersect transversally in a unique point. These graphs prove that the calculated solution is little sensitive to the approximation of physical parameters.

(37) the T_i values are the same. This result is another confirmation of the consistency of our model.

Based on the variation of k one can simply explain the Leidenfrost phenomenon as follows. If $k > 0$, the thermodynamic pressure p is lower in the vapor phase just near the liquid-vapor interface compared to the pressure p_0 near the surface. This results to a detachment of the liquid film from the surface. On the contrary, if $k < 0$, the thermodynamic pressure p is higher, and liquid film wets the surface causing a violent boiling. In fact the whole process is highly non-stationary and cannot be described by the stationary equations. However, our approach gives a reasonable estimation of the Leidenfrost temperature.

VII. CONCLUSION

For water, we study the boiling crisis phenomenon in the framework of the internal capillarity model.

A first important result is the capillary pressure term k allows us to understand the phenomenon and to determine the Leidenfrost temperature. The boiling crisis corresponds to $k > 0$, and Leidenfrost's temperature to $k = 0$. For water, the model predicts the Leidenfrost temperature which fairly agrees with experimental results. A second important result is the estimation of the temperature of liquid-vapor interface of water. It is proved that its value is below the

boiling temperature at atmospheric pressure. This result is also consistent with experimental data on the overall liquid temperature near the interface.

In the future, we plan to apply this model to other fluids for which all necessary experimental data are well documented.

Acknowledgments: The authors thank D. Brutin and B. Darbois-Textier for pointing out to us useful references, and the reviewers for a careful reading of the manuscript and for many helpful inquiries which allowed us to improve our paper. The authors are partially supported by Agence Nationale de la Recherche, France (SNIP ANR–19–ASTR–0016–01).

-
- [1] J. Walker, *The amateur scientist*, Scientific American, **237**, 126–131 (1977).
- [2] F. Celestini, T. Frisch, Y. Pomeau, *Take-Off of Small Leidenfrost Droplets*, Phys. Rev. Lett. **109**, 034501 (2012).
- [3] D. Quéré, *Leidenfrost dynamics*, Annu. Rev. Fluid. Mech. **45**, 197–215 (2013).
- [4] B. Darbois-Textier, G. Dupeux, G. Lagubeau, M. Le Merrer, K. Piroird, D. Soto, C. Clanet, D. Quéré, *La Caléfaction*, Reverts Phys. **37**, 12–16 (2013).
- [5] Y. Pomeau, M. Le Berre, F. Celestini, T. Frisch, *The Leidenfrost effect: From quasi-spherical droplets to puddles*, C. R. Mec. **340**, 867–881 (2012).
- [6] A.L. Biance, C. Clanet, D. Quéré, *Leidenfrost drops*, Physics of Fluids, **15**, 1632 (2003).
- [7] G. Graeber, K. Regulagadda, P. Hodel, C. Küttel, D. Landolf, T.M. Schutzius, D. Poulikakos, *Leidenfrost droplet trampolining*, Nature Communications, **124**, 1727 (2021).
- [8] S. Lyu, V. Mathai, Y. Wang, B. Sobac, P. Colinet, D. Lohse, C. Sun, *Final fate of a Leidenfrost droplet: Explosion or takeoff*, Sci. Adv. **5**, eaav8081 (2019).
- [9] B. Sobac, A. Rednikov, S. Dorbolo, P. Colinet, *Leidenfrost effect: Accurate drop shape modeling and refined scaling laws*, Physical Review E, **90**, 053011 (2014).
- [10] A. Bouillant, T. Mouterde, Ph. Bourriane, A. Lagarde, C. Clanet, D. Quéré, *Leidenfrost wheels (Supplementary Material: Temperature field inside Leidenfrost drops)*, Nature Physics, **14**, 1188–1192 (2018).
- [11] N.J. Holter, W.R. Glasscock, *Vibrations of evaporating liquid drops*, The Journal of the Acoustical Society of America, **24**, 682–686 (1952).
- [12] X. Ma, J.-J. Liéter-Santos, J.C. Burton, *Star-shaped oscillations of Leidenfrost drops*, Phys. Rev. Fluids, **2**, 031602(R) (2017).
- [13] P. Casal, H. Gouin, *Vibrations of liquid drops in film boiling phenomena*, International Journal Engineering Science, **32**, 1553–1560 (1994).
- [14] J. G. Leidenfrost. *De aquae communis nonnullis qualitibus tractatus*, Duisburg (1756); translated by C. Wares, *On the fixation of water in diverse fire*, Int. J. Heat Mass Transfer, **9**, 1153–1166 (1966).
- [15] M. Boutigny. *Sur les phénomènes que présentent les corps projetés sur des surfaces chaudes*, Annales de Chimie et Physique, **3**, IX 350–370 (1843); **3**, XI, 16–39 (1844).
- [16] J.C.A. Peltier. *Caléfaction* in: Grande Encyclopédie Méthodique, Universelle, Illustrée (Ed 1888), Hachette, B.N.F. (Bibliothèque Nationale de France, Paris, 2012).
- [17] J. D. Bernardin, I. Mudawar, *The Leidenfrost point: Experimental study and assessment of existing models*, J. Heat Transfer, **121**, 894–903 (1999).
- [18] P. Sadasivan, C. Unal, R. Nelson, *The need for new experiments*, J. Heat Transfer, **117**, 558–567 (1995).
- [19] P. Sadasivan, C. Unal, R. Nelson, *Nonlinear aspects of high heat flux nucleate boiling heat transfer*, J. Heat Transfer, **117**, 981–989 (1995).
- [20] G. Wang, J.R. McDonough, V. Zivkovic, T. Long, S. Wang, *From thermal energy to kinetic energy: droplet motion triggered by the Leidenfrost effect*, Review: Advanced Materials Interfaces, **8** (2), 2001249 (2021).
- [21] J.M. Delhaye, M. Giot, M.L. Riethmuller (eds.), *Thermohydraulics of Two-Phase Systems for Industrial Design and Nuclear Engineering* (Mc Graw-Hill, New York, 1981).
- [22] V.S. Nikolayev, D. Chatain, Y. Garrabos, D. Beysens, *Experimental Evidence of the Vapor Recoil Mechanism in the Boiling Crisis*, Phys. Rev. Lett. **97**, 184503 (2006).
- [23] P. Lloveras, F. Salvat-Pujol, L. Truskinovsky, E. Vives, *Boiling Crisis as a Critical Phenomenon*, Phys. Rev. Lett., **108**, 215701 (2012).
- [24] F. Celestini, T. Frisch, A. Cohen, C. Raufaste, L. Duchemin, Y. Pomeau, *Two dimensional Leidenfrost droplets in a Hele-Shaw cell*, Physics of Fluids, **26**, 032103 (2014).
- [25] T.Y. Zhaoa, N.A. Patankar, *The thermo-wetting instability driving Leidenfrost film collapse*, Proceedings of the National Academy of Sciences, **117**, 13321–13328 (2020).
- [26] M. Rein, *Interaction between drops and hot surfaces* in Drop–Surface Interactions, CISM Vol. **456**, p.p. 185–217 (Springer, Vienna, 2002).
- [27] M.A.J. van Limbeek, M.H.K. Schaarsberg, B. Sobac, A. Rednikov, C. Sun, P. Colinet, D. Lohse, *Leidenfrost drops cooling surfaces: theory and interferometric measurement*, J. Fluid Mech., **827**, 614–639 (2017).
- [28] M.A.J. van Limbeek, O. Ramirez-Soto, A. Properetti, D. Lohse, *How ambient conditions affect the Leidenfrost temperature*, Soft Matter, **17**, 3207–3218 (2021).
- [29] J.W. Cahn, J.E. Hilliard, *Free energy of a non-uniform system*, J. Chem. Phys., **31**, 688–699 (1959).
- [30] J.S. Rowlinson, B. Widom, *Molecular Theory of Capillarity*, (Clarendon Press, Oxford, 1984).
- [31] J. Rumble (Ed.) *Handbook of Chemistry and Physics, 102nd Edition*. (CRC Press, Boca Raton, FL, 2021).
- [32] N.C. Patel, A.S. Teja, *A new cubic equation of state for fluids and fluid mixtures*, Chem. Eng. Sciences, **37**, 463–473 (1982).
- [33] Y. Rocard, *Thermodynamique*, Masson, Paris (1967).
- [34] P. Germain, *The method of virtual power in the mechanics of continuous media, I: Second-gradient theory*, Mathematics and Mechanics of Complex Systems, **8**, No. 2, 153–190 (2020). Translated by M. Epstein and R.E. Smelser.
- [35] P. Casal, *La théorie du second gradient et la capillarité*, C.R. Acad. Sci. Paris, **274 A**, 1571–1574 (1972).
- [36] D.G. Triezenberg, R. Zwanzig *Fluctuation theory of surface tension*, Phys. Rev. Lett. **28**, 1183–1185 (2013).
- [37] B.V. Derjaguin, N.V. Churaev, V.M. Muller, *Surfaces Forces*. Springer, New-York (1987).
- [38] P.G. de Gennes, *Wetting: statics and dynamics*, Rev. Mod. Phys., **57**, 827–833 (1985).
- [39] P. Casal, *Principes variationnels en fluide compressible et en magnétodynamique des fluides*, Journal de Mécanique, **5**, 149–161 (1966).

- [40] H. Gouin, *Utilization of the second gradient theory in continuum mechanics to study the motions and thermodynamics of liquid-vapor interfaces*, in *Physicochemical Hydrodynamics*, edited by M. G. Velarde, NATO ASI Series B: Physics Vol. **174**, pp. 666–682 (Springer, Boston, MA, 1988).
- [41] S.L. Gavriluk, H. Gouin, *Rankine–Hugoniot conditions for fluids whose energy depends on space and time derivatives of density*, *Wave Motion*, **98**, 102620 (2020).
- [42] H. Gouin, *Rankine–Hugoniot conditions obtained by using the space–time Hamilton action*, *Ricerche di Matematica*, **70**, 115–129 (2021).
- [43] P. Casal, H. Gouin, *Connection between the energy equation and the motion equation in Korteweg’s theory of capillarity*, *C.R. Acad. Sci. Paris*, **300** (II), 231–234 (1985).
- [44] S. Gavriluk, B. Nkonga, K-M. Shyue, L. Truskinovsky, *Stationary shock-like transition fronts in dispersive systems*, *Nonlinearity*, **33**, 547–509 (2020).
- [45] S. Gavriluk, K-M. Shyue, *Singular solutions of the BBM equation: analytical and numerical study*, *Nonlinearity*, **35**, 388–410 (2022).
- [46] H. Gouin, W. Kosiński, *Boundary conditions for a capillary fluid in contact with a wall*, *Arch. Mech.* **50**, 907–916 (1998).
- [47] B.S. Gottfried, C.J. Lee, and K.J. Bell, *The Leidenfrost phenomenon: Film boiling of liquid droplets on a flat plate*, *Int. J. Heat Mass Transf.* **9**, 1167–1188 (1966).
- [48] A-L. Himbert-Biance, *Gouttes inertielles: de la caléfaction à l’étalement*, PhD thesis, Sorbone University (2005).
- [49] A.S. Rana, D.A. Lockerby, J.E. Sprittles, *Lifetime of a Nanodroplet: Kinetic Effects and Regime Transitions*, *Phys. Rev. Lett.* **123**, 154501 (2019).
- [50] E.W. Lemmon, M.L. Hubert, M.O. McLinden, *NIST Standard Reference Database 23: Reference Fluid Thermodynamic and Transport Properties–REFPROP Version 9.0*, National Institute of Standards and technology, Standard Reference Data Program, Gaithersburg, Maryland (2010). (www.nist.gov/srd/nist23.cfm)
- [51] G. Liang, I. Mudawar, *Review of drop impact on heated walls*, *Int. J. Heat Mass Transfer*, **106**, 103–126 (2017).
- [52] P. Bourrienne, C. Lv, D. Quééré, *The cold Leidenfrost regime*, *Sci. Adv.* **5**, eaaw0304 (2019).
- [53] L. Maquet, B. Sobac, B. Darbois-Texier, A. Duchesne, M. Brandenbourger, A. Rednikov, P. Colinet, S. Dorbolo, *Leidenfrost drops on a heated liquid pool*, *Physical Review Fluids*, **1**, 053902 (2016).
- [54] N. Tokugawa, R. Takaki, *Mechanism of self-induced vibration of a liquid drop based on the surface tension fluctuation*, *J. Phys. Soc. Jpn.* **63**, 1758–1768 (1994).

Appendix A: Extra-condition at dynamical liquid-vapor interfaces

Extra-condition (19) does not come from conservation laws. It is a natural boundary condition coming from Lagrangian formulation of the problem. It already appeared in the study of discontinuous solutions of dispersive equations [41, 44, 45]. To give a proof in the one-dimensional case, we consider a general action functional:

$$\mathcal{A}\{y\} = \int_I \mathcal{L}(y, y') dx,$$

$y(x)$ is an unknown function, and the integral is taken over a finite interval I . The values of $y(x)$ are fixed at the ends of interval I . We are looking for $y(x)$ on which the functional is extremal and we do not assume that $y(x)$ is smooth. The variation of Hamilton’s action \mathcal{A} can be written as:

$$\delta\mathcal{A} = \int_I \left\{ \frac{\delta\mathcal{L}}{\delta y} \delta y + \frac{d}{dx} \left(\frac{\partial\mathcal{L}}{\partial y'} \delta y \right) \right\} dx,$$

$$\text{with } \frac{\delta\mathcal{L}}{\delta y} = \frac{\partial\mathcal{L}}{\partial y} - \frac{d}{dx} \left(\frac{\partial\mathcal{L}}{\partial y'} \right).$$

In the case of non-smooth (or “broken”) extremal curves, the same Euler–Lagrange equation should be satisfied for each smooth part of the extremal curve:

$$\frac{\delta\mathcal{L}}{\delta y} = 0. \quad (\text{A1})$$

Together with Eq. (A1) an additional condition should also be satisfied at the “broken” point:

$$\left[\frac{\partial\mathcal{L}}{\partial y'} \right] = 0. \quad (\text{A2})$$

In the case of capillary fluids, \mathcal{L} is quadratic with respect to y' because λ is constant. It implies that y' is continuous at the broken point. Condition (A2) is usually called *Weierstrass-Erdmann* condition, or *corner* condition. In particular, if a piecewise C^2 -solution $y(x)$ is constant on some interval of x , but is not constant on a neighboring interval, this solution should have a zero slope at the broken point.

Appendix B: Special cases of capillary fluid motion

1. Isothermal motion

In the case of isothermal stationary motion, the whole entropy of domain \mathcal{D}_t corresponding to the bulk (a) and interface (i) is:

$$\int_{\mathcal{D}_t} \rho\eta dD = S_0, \quad (\text{B1})$$

where S_0 is constant (independent of time t), and dD is the infinitesimal volume. Due to constraint (B1), Hamilton’s action is modified into the following: there exists a constant Lagrange multiplier T_0 such that the new Lagrangian \mathcal{L} is associated with $\alpha - T_0\eta$ which is the specific free energy at constant temperature. The application of the Hamilton principle yields the same equations of motion where α has to be replaced by $\alpha - T_0\eta$. Consequently, the specific enthalpy is replaced by the chemical potential μ . The variation of η implies $T - T_0 = 0$.

2. Motion at constant pressure

In the case of stationary motion, if domain \mathcal{D}_t is an invariant control volume through which the steam flows, it verifies:

$$\int_{\mathcal{D}_t} dD = \mathcal{V}_0, \quad (\text{B2})$$

where \mathcal{V}_0 is constant (independent of time t). Due to constraint (B2), Hamilton's action is modified into the following: there exists a constant Lagrange multiplier p_0 such that the new Lagrangian \mathcal{L} is associated with $\mathcal{H} = \alpha + p_0/\rho$, which is the specific enthalpy of capillary fluid at constant pressure p_0 . Consequently, in Subsection III A, in the energy equation, the specific energy should be replaced by the specific enthalpy at constant pressure p_0 , and the equation of motion is unchanged.

Appendix C: Isothermic oscillations of the vapor density near liquid-vapor interface (i)

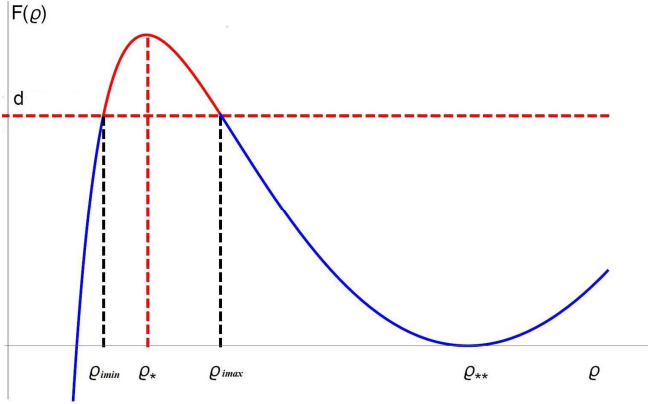


FIG. 7. If $M_i^2 < 1$, the curve $F(\rho)$ has a local maximum at $\rho_* \in]\rho_{imin}, \rho_{imax}[$, and a local minimum at $\rho_{**} \in]\rho_{imax}, +\infty[$. We recall that $\rho = \rho_{**}$ is a formal value of ρ and that the physical part of the curve is only the red part of $F(\rho)$ corresponding to oscillations of density between ρ_{imin} and ρ_{imax} .

We look for oscillating stationary vapor flow in the immediate vicinity of interface (i) where the temperature is T_i . The governing equation of motion in the vapor phase is deduced from Eqs (11) and (12), and writes in the form:

$$\lambda \frac{d^2 \rho}{dx^2} = \mu(\rho, T_i) + \frac{q^2}{2\rho^2} + r,$$

where r is a constant of integration. The vapor is considered as an ideal gas; we get the potential μ , defined up to an additive constant which can be included in r :

$$\mu(\rho, T_i) = c_{T_i}^2 \text{Log } \rho, \quad \text{where } c_{T_i}^2 = \mathcal{R}T_i.$$

Here c_{T_i} denotes the isothermal sound velocity of vapor at temperature T_i . To obtain oscillatory solutions, we choose a special value of r replacing it by a new constant ρ_{**} :

$$\lambda \frac{d^2 \rho}{dx^2} = c_{T_i}^2 \text{Log} \left(\frac{\rho}{\rho_{**}} \right) + \frac{q^2}{2\rho^2} - \frac{q^2}{2\rho_{**}^2}. \quad (\text{C1})$$

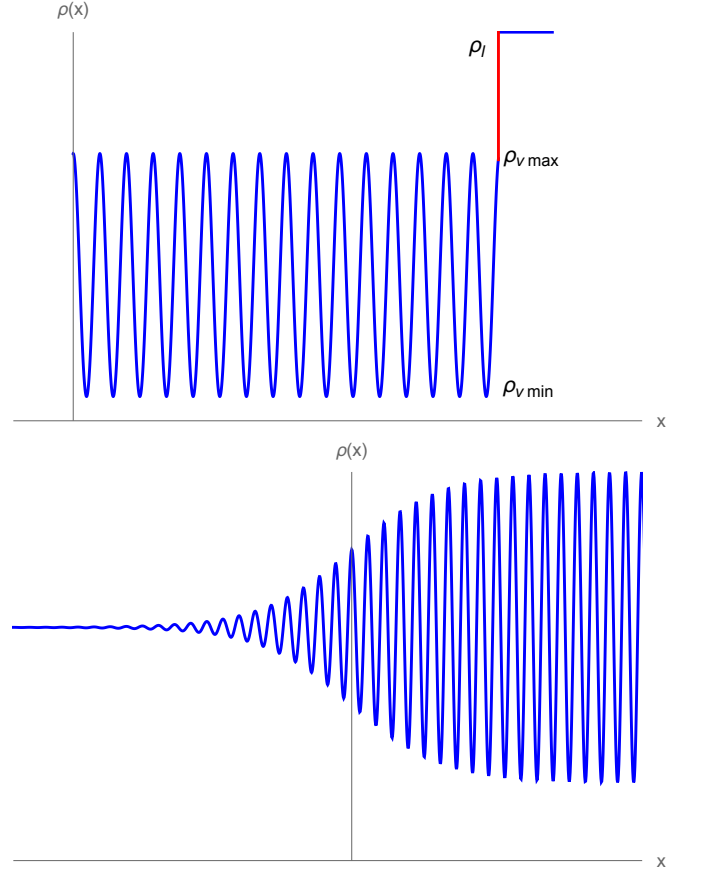


FIG. 8. Upper figure : The vapor density oscillates near the isothermal liquid-vapor interface. At the interface the density jumps (and decreases) from $\rho_l = 1/v_{li}$ to $\rho_{gl} = 1/v_{gli}$. The vapor density being oscillating between two extrema ρ_{imin} and ρ_{imax} where $d\rho/dx = 0$, we have to choose between these two values. The jump from ρ_l to ρ_{imax} has a smaller amplitude compared to that from ρ_l to ρ_{imin} , and hence a smaller energy decrease. Consequently, $d^2\rho/dx^2 < 0$ when $\rho_{vi} = \rho_{imax}$ and $k = -\lambda\rho d^2\rho/dx^2 > 0$. Bottom figure : case of dissipative vapor flow. The oscillations of vapor density vanish near the surface boundary layer.

Integrating Eq. (C1), one obtains:

$$\frac{\lambda}{2} \left(\frac{d\rho}{dx} \right)^2 = F(\rho) - d, \quad \text{where } d = \text{const.} \quad (\text{C2})$$

with

$$F(\rho) = c_{T_i}^2 \left(\rho \text{Log} \left(\frac{\rho}{\rho_{**}} \right) - \rho + \rho_{**} \right) - \frac{q^2}{2\rho} \left(1 - \frac{\rho}{\rho_{**}} \right)^2.$$

By construction,

$$F(\rho_{**}) = 0, \quad \frac{dF}{d\rho}(\rho_{**}) = 0.$$

The variation of F for the Mach number $M_i^2 = q^2/(\rho_{**} c_{T_i})^2 < 1$ is shown in Fig.7 (In liquid water $\rho_l \approx 10^3 \text{ kg/m}^3$. If boiling-evaporation time of a liquid film with 10^{-2} m thickness is

about 100 s; then $u \approx 10^{-4} \text{ m/s}$ and for the liquid, the flow rate $q \approx 10^{-1} \text{ kg/m}^2 \cdot \text{s}$. In the vapor $\rho_l \approx 1 \text{ kg/m}^3$ and consequently $u \approx 10^{-1} \text{ m/s}$, and $M_l^2 \approx 10^{-7} < 1$. It has a unique maximum point ρ_* such that $0 < \rho_* < \rho_{**}$. Moreover, $F \rightarrow -\infty$ as $\rho \rightarrow +0$. Hence, for any d such that $0 < d < F(\rho_*)$ one has a solution of (C2) oscillating between ρ_{imin} and ρ_{imax} , where $F(\rho_{imin}) = F(\rho_{imax}) = d$ (see Fig. 7). The solution of (C2) is schematically shown in Fig. 8 (on the high diagram). The liquid–vapor interface is considered as a discontinuity. So, the density jumps from ρ_{li} to the extreme value of the vapor density (see the extra condition (19)). Since we have two possible

values (minimum and maximum values), the choice has to be done. Obviously, the jump from ρ_{li} to ρ_{imax} has a smaller amplitude compared to that from ρ_{li} to ρ_{imin} , and hence the smallest energy variation. Also, physically, only this choice allows us to obtain ‘levitation’ of the liquid film. Such a stationary periodic solution gives us an idea about a strong density variation near the interface: the liquid–vapor interface is endowed with a micro-structure representing a strongly oscillatory region. The vapor region represents a transition zone that begins with an oscillatory regime and ends with a region of homogeneous density (see the bottom diagram in Fig. 8).